Chinese Journal of Aeronautics, 2013,26(3): 823–830

Chinese Society of Aeronautics and Astronautics
& Beihang University

Chinese Journal of Aeronautics

cja@buaa.edu.cn
www.sciencedirect.com

Mechanistic identification of cutting force coefficients in bull-nose milling process

Gao Ge, Wu Baohai, Zhang Dinghua *, Luo Ming

The Key Laboratory of Contemporary Design and Integrated Manufacturing Technology, Ministry of Education, Northwestern Polytechnical University, Xi'an 710072, China

Received 8 March 2012; revised 21 April 2012; accepted 17 July 2012
Available online 28 April 2013

KEYWORDS

Bull-nose cutter;
Calibration;
Cutting force;
Cutting force coefficient;
Mechanistic model

Abstract An improved method to determine cutting force coefficients for bull-nose cutters is proposed based on the semi-mechanistic cutting force model. Due to variations of cutting speed along the tool axis in bull-nose milling, they affect coefficients significantly and may bring remarkable discrepancies in the prediction of cutting forces. Firstly, the bull-nose cutter is regarded as a finite number of axial discs piled up along the tool axis, and the rigid cutting force model is exerted. Then through discretization along cutting edges, the cutting force related to each element is recalculated, which equals to differential force value between the current and previous elements. In addition, coefficient identification adopts the cubic polynomial fitting method with the slice elevation as its horizontal axis. By calculating relations of cutting speed and cutting depth, the influences of speed variations on cutting force can be derived. Thereby, several tests are conducted to calibrate the coefficients using the improved method, which are applied to later force predictions. Eventually, experimental evaluations are discussed to verify the effectiveness. Compared to the conventional method, the results are more accurate and show satisfactory consistency with the simulations. For further applications, the method is instructive to predict the cutting forces in bull-nose milling with lead or tilt angles and can be extended to the selection of cutting parameters.

1. Introduction

Bull-nose cutters have been applied to manufacturing of complicated parts with free-form surfaces extensively, where cutting force acts as an essential parameter. It is the basis for judging the deflection, vibration of tool-workpiece system, tool wear, breakage, tool life span, and surface integrity of machined parts.[1–5] Meanwhile, it is recognized that the quantity and distribution of milling forces are significantly affected by dynamic factors especially in multi-fluted operations. So far, considerable studies have been conducted in accurate force predictions with various cutter and test types.

According to early studies,[3–8] cutting force predictions are mainly characterized by three methods: analytical, mechanistic, and numerical methods. However, the first model has less accuracy and the third is time-consuming. The second one gives intermediate advantages based on different cutting conditions and cutter types. Cheng and Tsay[1] established

* Corresponding author. Tel.: +86 29 88493009.
E-mail addresses: gaogeflying@163.com (G. Gao), dhzhang@nwpu.edu.cn (D. Zhang).

Peer review review under responsibility of Editorial Committee of CJA.

1000-9361 © 2013 Production and hosting by Elsevier Ltd. on behalf of CSAA & BUAA. Open access under CC BY-NC-ND license.
http://dx.doi.org/10.1016/j.cja.2013.04.007

relationships between instantaneous cutting force coefficients and other cutting parameters, and analyzed different degrees of influential factors. Gonzalo and Beristain[2] introduced an inverse method to instantaneous cutting force calculation by solving relative equations and explained the influences of rake angle and chip thickness on cutting coefficients. Additionally, a convolution integral approach was utilized to contrive the shearing and ploughing cutting constants with average cutting forces. Then it was precisely verified through experiments by being compared with the accuracy of lumped cutting force model in ball-end milling.[3] Wan and Zhang[4] put forward a calibration method of instantaneous cutting force coefficients based on the lumped force model for general end mills. Similar works have also been done on identification of dynamic cutting force coefficients considering the influences of regenerative chip thickness, velocity, process damping, etc.[5] Later, a cutting force prediction method and derived algorithm made it possible to determine cutting force coefficients without restrictions in cutting geometry.[6] Currently, another interest in machining process modeling is the finite element method (FEM) based on specific software that provides simulation functionalities with different helical mills.[7]

Most of the mentioned works focus on different cutting force models and cutter types in the process of cutting force coefficient identification. However, the calibration is either inaccurate with low practicability, or just suitable for certain tool types. Additionally, the influences of cutting speed variations along the tool axis are not taken into the force modeling or coefficient identification processes. The goal of this research is to present an improved calibration approach based on a semi-mechanical force model. During the process, cutting force on each disc is recalculated corresponding to its elevation z for bull-nose milling. By doing this, the identification procedure is improved which incorporates the influences of different cutting speeds along the tool axis. Then, cutting force comparisons supported by tests are made to illustrate the validity of the improved method compared with the conventional approach. The method shows good computational efficiency, and force predictions are proved in good agreement with measured data. According to analysis, the presented identification method can be further extended to predict cutting forces in tool-workpiece inclination conditions, which is part of the ongoing endeavor.

2. Computation scheme

2.1. Geometry of bull-nose cutter

The envelope of a bull-nose cutter is derived from the generalized end mill model. By assigning certain values to seven parameters D, R, R_r, R_z, α, β and h defined in a generic tool,[4] the bull-nose mill[8,9] can be obtained in Fig. 1. To facilitate computations, two separated zones are divided: the toroidal surface $\overset{\frown}{MN}$ with variable helical angles and surface NS with constant lead resembling cylindrical tools, respectively.

Cutting speed varies along the cutting flute in the $\overset{\frown}{MN}$ zone of a bull-nose cutter, which affects force predictions significantly. Meanwhile, chip load, instantaneous undeformed chip thickness, and cutting force components should be identified to evaluate cutting forces acting on each cutting edge wrapped around the cutter contour. The geometry of a tool can be regarded as a finite number of axial discs piled up along the tool axis. Since the cutting force varies in different discs, for each horizontal layer, the force is regarded as an independent element. Then the total one can be obtained through integration along the tool axis. From previous literature,[10–12] three cutting force components (tangential, axial, and radial) can be expressed as

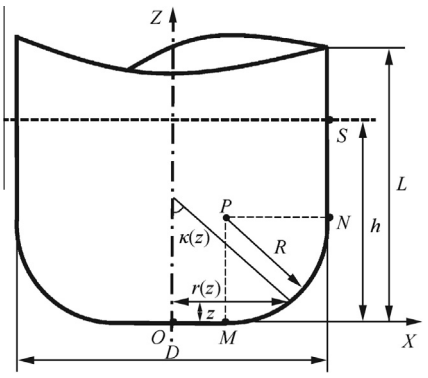

Fig. 1 Geometry of the bull-nose cutter.

$$\begin{cases} \mathrm{d}F_{\mathrm{t},j}(\phi,z) = K_{\mathrm{tc}}h_{i,j}(z)\mathrm{d}b + K_{\mathrm{te}}\mathrm{d}s \\ \mathrm{d}F_{\mathrm{r},j}(\phi,z) = K_{\mathrm{rc}}h_{i,j}(z)\mathrm{d}b + K_{\mathrm{re}}\mathrm{d}s \\ \mathrm{d}F_{\mathrm{a},j}(\phi,z) = K_{\mathrm{ac}}h_{i,j}(z)\mathrm{d}b + K_{\mathrm{ae}}\mathrm{d}s \end{cases} \tag{1}$$

In order to clearly represent and calculate related parameters, a coordinate system is established with its X-axis tangent to the feed direction and Z-axis parallel to the tool axis. Therefore, the vector from the cutter tip to an arbitrary point on the cutting edge can be written as

$$\boldsymbol{r}_j = x_j\boldsymbol{i} + y_j\boldsymbol{j} + z_j\boldsymbol{k} = r(\varphi_j)(\sin\varphi_j\boldsymbol{i} + \cos\varphi_j\boldsymbol{j}) + z(\varphi_j)\boldsymbol{k} \tag{2}$$

where φ_j refers to the radial immersion angle on the jth cutting edge at the elevation z. As the cutter rotates, its helical angle and radial immersion angle change too. Suppose the first cutting edge $j = 1$ to be the reference edge and its helical angle at elevation $z = 0$ to be φ, so the radial immersion angle of the jth cutting edge at elevation z is shown as

$$\varphi_j(z) = \varphi + \sum_{n=1}^{j}\varphi_{\mathrm{pj}} - \psi(z) \tag{3}$$

where φ_{pj} is the pitch angle defined as $\varphi_{\mathrm{pj}} = 2\pi/N$ and $\psi(z)$ represents the radial lag angle caused by the local helical angle. It is necessary to calculate the undeformed chip thickness based on the analysis of cutter geometric modeling and kinematics. If the position of one cutting edge is defined, the undeformed chip thickness is expressed according to the radial and axial immersion angles

$$h(\phi_j) = s_{\mathrm{tj}}\sin\phi_j\sin\kappa \tag{4}$$

where s_{tj} ($s_{\mathrm{tj}} = 60v/(Nn)$) is the feed per tooth, v means the feed velocity, and n represents the spindle rotation speed (rpm). Additionally, ϕ_j and κ refer to the radial and axial immersion angles, respectively. According to the periphery features of a bull-nose cutter, the analytic expressions of two subdivided zones are shown

$$\begin{cases} r(z) = \frac{D}{2} - R + \sqrt{R^2 - (R-z)^2} & \text{zone } \overset{\frown}{MN} \\ r(z) = \frac{D}{2} & \text{zone } \overset{\frown}{NS} \end{cases} \tag{5}$$

In cutter manufacturing industries, some bull-nose cutters have a constant helical angle, while some with a constant lead that makes the grinding process much simpler. The helix on a bull-nose cutter resembles consequences of projecting a helical line onto the toroidal surface along the direction which is vertical to the tool axis. The helical angle varies along the flute due to the changing radial radius in the MN zone. While i_0 is the invariable helical angle in the cylindrical part, $i(z)$ refers to the changing angle in the toroidal zone and is defined as

$$i(z) = \tan^{-1}\left[\frac{(r(z) - R_r)\tan i_0}{R}\right] \tag{6}$$

where $r(z)$ is the cutter radius at elevation z, and R is the circular radius. The arc MN is tangent to OM and NS with its circle center at point P, a radial offset of R_r and the arc radius of R. Therefore, the cutter profile reaches tangential continuous, and the lag angle is the function of elevation z. The radial offset at elevation z and the axial immersion angle $\kappa(z)$ located in different zones can be expressed as

$$\begin{cases} \psi(z) = \frac{z}{R}\tan i_0 \quad \kappa(z) = \arccos\frac{R-z}{R} & \text{zone } \overset{\frown}{MN} \\ \psi(z) = \frac{2z\tan i_0}{D} \quad \kappa(z) = \frac{\pi}{2} & \text{zone } \overset{\frown}{NS} \end{cases} \tag{7}$$

2.2. Mechanistic cutting force model

Cutting forces are modeled in terms of two fundamental factors: shearing effects taking place in the shear zone and edge effects induced by plowing or ploughing at cutting edges. Six force coefficients need to be identified through experiments and mathematical analysis for a particular cutter vs. workpiece material under specific cutting conditions. Then cutting force is attained with the information of six coefficients, undeformed chip thickness, etc. Meanwhile, the current model focuses on dividing a cutting edge into small discrete discs and applying mathematical formulations to each element. After the calculation of cutting force on each element, resultant force is the summation of all the units on each cutting edge. The adopted model is based on a previous study by Lee and Altintas.[13]

Three differential force components acting on the infinitesimal cutting edge segment can be expressed as $dF_{s,j} = K_{sc}h_{i,j}db + K_{se}ds(s = t, r, a)$, where K_{se} and K_{sc} are the cutting coefficients related to edge rubbing and chip shearing mechanisms, respectively. $h_{i,j}$ refers to the instantaneous undeformed chip thickness. Cutting width db ($db = dz/\sin\kappa(z)$) is the projected length of an infinitesimal cutting flute along the direction of cutting velocity shown in Fig. 2. ds can be derived from Eq. (8) which is relevant to the elevation z and defined as the edge length of the current engaged element.[14]

$$ds(z) = dz\sqrt{(r(z)\psi'(z))^2 + (r'(z))^2 + 1} \tag{8}$$

As the cutter rotates, cutting force components on every slice are calculated by discretizing cutting flutes into infinite elements. After obtaining tangential, radial, and axial cutting force components by integrating, the forces in a Cartesian coordinate system are derived through coordinate transformation from orthogonal to oblique cutting. The forces for multi-fluted cutters can be obtained by summing the forces acting on individual flutes in the cut. The mapping of cutting forces is shown as

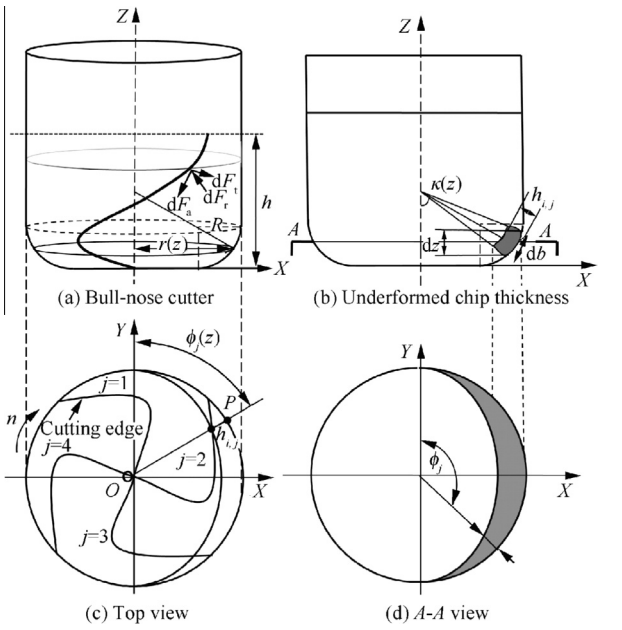

Fig. 2 Immersion angle, cutting force components, cutting width, and chip load at point P in a bull-nose end mill.

$$\begin{bmatrix} F_{i,j,x} \\ F_{i,j,y} \\ F_{i,j,z} \end{bmatrix} = \boldsymbol{T}\begin{bmatrix} F_{i,j,t} \\ F_{i,j,r} \\ F_{i,j,a} \end{bmatrix} \tag{9}$$

where

$$\boldsymbol{T} = \begin{bmatrix} -\cos\phi_{i,j} & -\sin\kappa\sin\phi_{i,j} & -\cos\kappa\sin\phi_{i,j} \\ \sin\phi_{i,j} & -\sin\kappa\cos\phi_{i,j} & -\cos\kappa\cos\phi_{i,j} \\ 0 & \cos\kappa & -\sin\kappa \end{bmatrix}$$

2.3. Identification of specific force coefficients

A vast of geometric parameters should be determined such as shearing angle, shearing strength, and friction index when using the identification method of friction and pressure loads on the rake face.[15] These factors could bring uncertain effects and the determination procedure could be sophisticated. Thus, an improved semi-mechanistic method with higher accuracy is adopted. It is assumed that the average cutting forces from experiments are the input factors to derive cutting force coefficients. The illustration of the analytical equation for average cutting force is

$$F = \frac{1}{\phi_p}\int_{\phi_{st}}^{\phi_{ex}}\int_0^{z_1} dF d\phi \tag{10}$$

where ϕ_{st} and ϕ_{ex} represent the start and exit angles, respectively. The axial integration limits for each flute are determined from the cutter-workpiece engagement area. In slot millings, $\phi_{st} = 0$, $\phi_{ex} = \pi$. Since the cutting material removed is constant in one cutter tooth period regardless of helical angles,

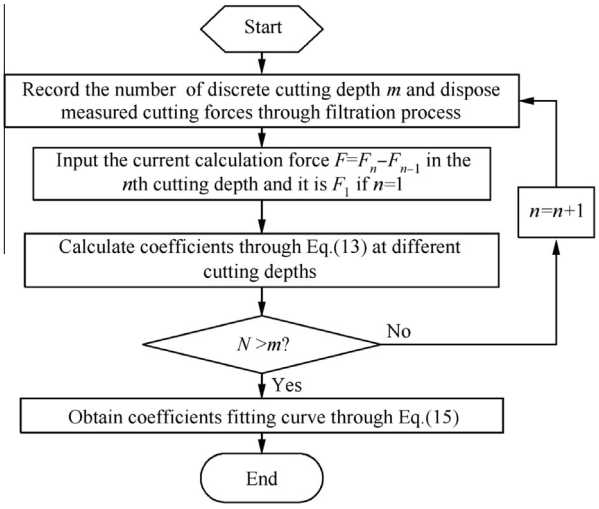

Fig. 3 Flowchart of the identification process.

the magnitude of average cutting force is irrelevant with helical angle. Therefore, instantaneous cutting forces can be derived with the assumption that β is equal to zero

$$\begin{bmatrix} F_x(\phi) \\ F_y(\phi) \\ F_z(\phi) \end{bmatrix} = \frac{1}{2} s_{tj} \boldsymbol{T}_1 \begin{bmatrix} a_1 \\ a_2 \\ a_3 \end{bmatrix} + \boldsymbol{T}_2 \begin{bmatrix} b_1 \\ b_2 \\ b_3 \end{bmatrix} \tag{11}$$

where ϕ refers to the radial immersion angle and

$$\boldsymbol{T}_1 = \begin{bmatrix} -K_{tc}\sin(2\phi) & -K_{rc}\sin^2\phi & -K_{ac}\sin^2\phi \\ 2K_{tc}\sin^2\phi & -K_{rc}\sin(2\phi) & -K_{ac}\sin(2\phi) \\ 0 & -2K_{ac}\sin\phi & 2K_{rc}\sin\phi \end{bmatrix}$$

$$\boldsymbol{T}_2 = \begin{bmatrix} -K_{te}\cos\phi & -K_{re}\sin\phi & -K_{ae}\sin\phi \\ K_{te}\sin\phi & -K_{re}\cos\phi & -K_{ae}\cos\phi \\ 0 & -K_{ae} & -K_{re}\cos\phi \end{bmatrix}$$

Elements a_s and b_s $(s = 1, 2, 3)$ are the constants determined by the cutter geometry.[16] A case in point is that if the cutting depth exceeds the circular radius, integral equations differ in upper and lower bounds. Otherwise, by substituting Eq. (2) into Eq. (1), the prediction derivation of cutting forces is illustrated as

$$\begin{bmatrix} \bar{F}_x \\ \bar{F}_y \\ \bar{F}_z \end{bmatrix} = \frac{s_{tj}}{\phi_p} \boldsymbol{C} \begin{bmatrix} K_{tc} \\ K_{rc} \\ K_{ac} \end{bmatrix} + \frac{1}{\phi_p} \boldsymbol{D} \begin{bmatrix} K_{te} \\ K_{re} \\ K_{ae} \end{bmatrix} \tag{12}$$

The matrices $\boldsymbol{C}$ and $\boldsymbol{D}$ depend on process parameters such as the cutter geometry, radial immersion angle, and cutting depth, and two separate integration parts are required to determine the matrix constants. These two independent integral parts are related to the start and exit angles as well as the axial depth of cut. By applying the linear fitting method in a range of different feed rates, it makes coefficient-related values in a certain cutting depth available. Then cutting force coefficients with respect to any elevation z can be obtained through experimental data and a non-linear fitting method. Identification experiments adopt slot milling with the bull-nose cutter to simplify calculations.

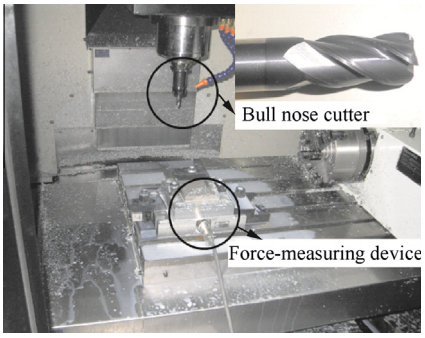

Fig. 4 Experimental setup.

After getting the measured average cutting forces of different feed rates at constant radial and axial cutting depths, two corresponding data are fitted through linear approximation. One degree item is the matrix related to specific cutting coefficients, while the constant item is associated with edge force coefficients under a certain cutting depth.

The expressions provide factors to solve six coefficients at any elevation. Geometric constants are defined by Eq. (13), while the integrant is characterized by the value of the cutting depth.

$$\begin{cases} a_1 = \int_{z_1}^{z_2} \mathrm{d}z, a_2 = \int_{z_1}^{z_2} \sin\kappa(z)\mathrm{d}z, a_3 = \int_{z_1}^{z_2} \cos\kappa(z)\mathrm{d}z \\ b_1 = \int_{z_1}^{z_2} \mathrm{d}s, b_2 = \int_{z_1}^{z_2} \sin\kappa(z)\mathrm{d}s, b_3 = \int_{z_1}^{z_2} \cos\kappa(z)\mathrm{d}s \\ K = \frac{1}{\phi_p} \begin{bmatrix} \boldsymbol{T}_3 & 0 \\ 0 & \boldsymbol{T}_4 \end{bmatrix} \boldsymbol{T}_5 \end{cases} \tag{13}$$

with

$$\boldsymbol{T}_3 = \begin{bmatrix} 0 & \frac{-\pi a_2}{2} & \frac{-\pi}{2} a_3 \\ \frac{\pi a_1}{2} & 0 & 0 \\ 0 & 2a_3 & -2a_2 \end{bmatrix}; \boldsymbol{T}_4 = \begin{bmatrix} 0 & -2b_2 & -2b_3 \\ 2b_1 & 0 & 0 \\ 0 & \pi b_3 & -\pi b_2 \end{bmatrix}$$

Matrix $\boldsymbol{T}_5$ with 6×1 elements is a combination of linear and constant items in the linear fitting procedure. Suppose the discrete cutting depths in experiments are $\{x_1, x_2, x_3, x_4, x_5, x_6\}$ with the feed rates of $\{s_1, s_2, s_3, s_4, s_5\}$, and $\{F_1, F_2, \ldots, F_6\}$ is the parallelism cutting forces. While F in Eq. (12) at different depths should be changed into $\bar{F}_s = \bar{F}_{s,n} - \bar{F}_{s,n-1}$ $(s = x, y, z)$, n is the current cutting depth and $n-1$ refers to the previous depth. Since the cutting force components are in three axes, each element of $\{F_1, F_2, \ldots, F_6\}$ has three components as well. The force on each span is recalculated based on the forces on the current and adjacent layers. Taking one force component in the x direction as an example, the cutting forces adopted in different discs are

Table 1 Tool parameters.

Item	Tool diameter (mm)	Arc radius (mm)	Cutting edge height (mm)	Toolholder height (mm)	Teeth No.
Value	10	2	20	75	4

$$\begin{bmatrix} F_{x_1} \\ F_{x_2} - F_{x_1} \\ F_{x_3} - F_{x_2} \\ \cdot \\ \cdot \\ \cdot \\ F_{x_n} - F_{x_{n-1}} \end{bmatrix} = \begin{bmatrix} F_1 \\ F_2 \\ F_3 \\ \cdot \\ \cdot \\ \cdot \\ F_n \end{bmatrix} \tag{14}$$

where $\{F_1, F_2, \ldots, F_6\}$ are the input elements of Eq. (14) which are considered as the cutting forces in the $\{1, 2, 3, \cdots, n\}$th disc. Cutting force coefficients are the differential value corresponding to each elevation span. Therefore, the improved method makes the force prediction more reliable and accurate by incorporating the influences of cutting speed variations. It also proves that the coefficients are effective and fit well with the measured data through cubic polynomial fitting. The detailed expression can be written as

$$K = ax^3 + bx^2 + cx + d \tag{15}$$

where polynomial coefficients a, b, c, d are determined by experimental data. In Eq. (15), x refers to the distance along z-axis. The final expressions of cutting force coefficients K can be obtained through cubic polynomial fitting. The entire flowchart of the identification process is listed in Fig. 3.

The accuracy of this identification method is somewhat related to test number and fitting order, while a cutting depth interval of 0.2 mm and cubic polynomial fitting is sufficient. FAM (Flute Average Method) is also applied to eliminate cutter runout effects by averaging sampled points.

3. Simulation and experimental results

In order to obtain cutting force coefficients in bull-nose milling processes, a series of slot milling experiments are conducted. The workpiece material is Al-7075 and performed on a 3-axis milling machine. The force-measure device is a Kistler 9255B dynamometer shown in Fig. 4. A tool of 12 mm in diameter is used with 4 evenly spaced teeth and a certain helical angle of 45 degrees in the cylindrical section as well as 2 mm arc radius, as shown in Table 1. Cutting parameters are as follows: spindle speed is 3000 rpm, and a series of feed rates with 0.02, 0.04, 0.06, 0.08, 0.10 mm/tooth are applied under the cutting depth group 0.2, 0.4, 0.6, 0.8, 1.0, 1.2, 1.4 mm. Since spindle rotary velocity remains in the stable zone which is chosen according to stability lobe diagram in literature,[17,18] the dynamic influences such as vibration or chatter on milling process plays a slight role. At a certain cutting depth, full immersion experiments are repeated in every feed rate with the combination of the other fixed parameters.

Cutting coefficients should be defined under specific conditions. As they influence cutting forces dramatically, different identification methods may have varying resultant forces. Fig. 5 gives force comparisons between theoretical data from the conventional identification method and measured data under two cutting depths. The black ellipses marked in Fig. 5(a and c) refer to the sampled data in Fig. 5(b and d).

It is evident from contrasts in Fig. 5, the conventional method has a relatively accurate force prediction particularly in x-axis, whereas, the force deviation remains large to some extent in Cartesian directions y and z. Predicted forces vary slightly while measured ones show periodic fluctuations during the cutter rotation. Only F_y at a 0.6 mm cutting depth gives

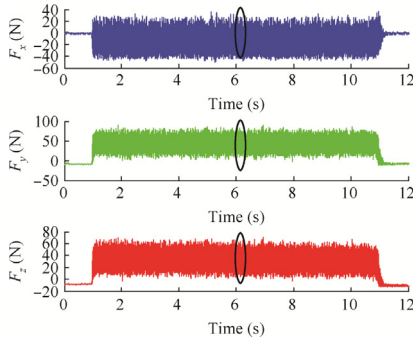

(a) Real measured cutting forces in cutting depth 0.4 mm

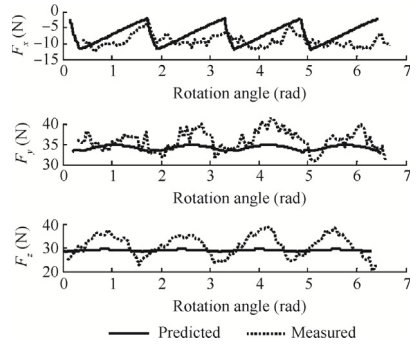

(b) Cutting depth 0.4 mm

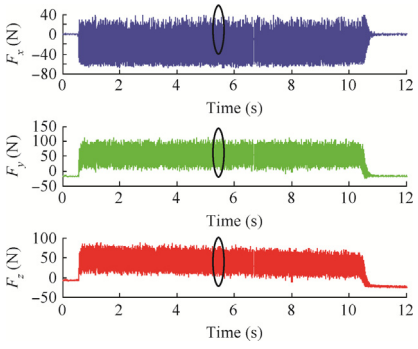

(c) Real measured cutting forces in cutting depth 0.6 mm

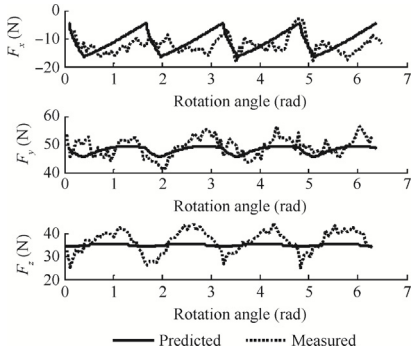

(d) Cutting depth 0.6 mm

Fig. 5 Comparison of cutting forces by using conventional coefficients identification method, $s_{tj} = 0.04$ mm/tooth.

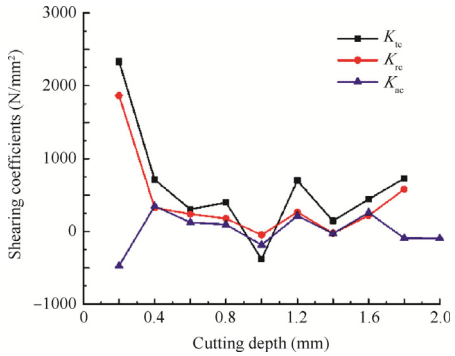

(a) Experimental data of shearing coefficients

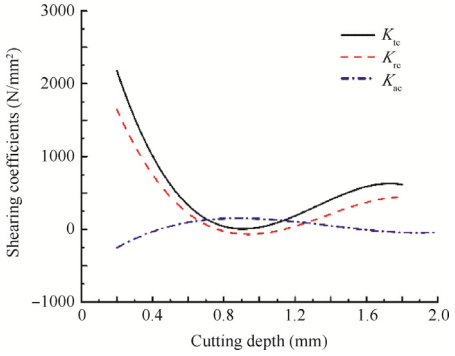

(b) Fitting of shearing coefficients

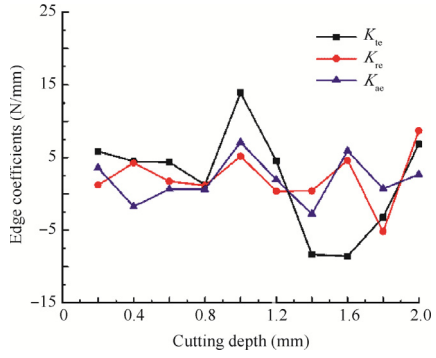

(c) Experimental data of edge coefficients

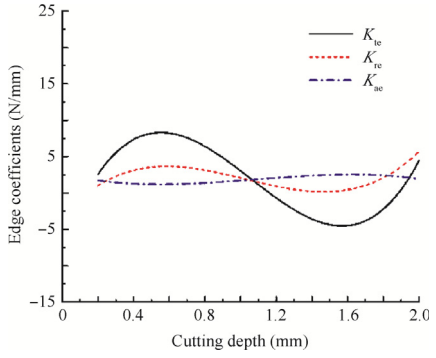

(d) Fitting of edge coefficients

Fig. 6 Cutting force coefficient identification using pro-posed method.

satisfactory coherence with experiments by keeping the error in a small range. From the whole perspective, the traditional

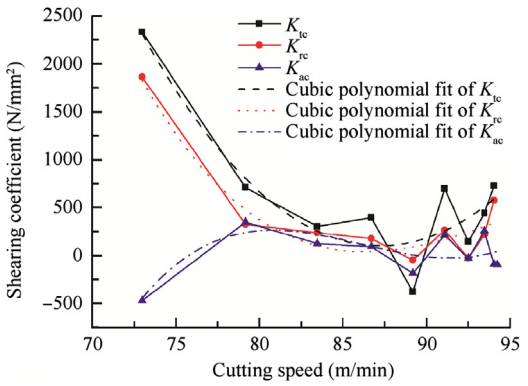

(a) Shearing coefficients

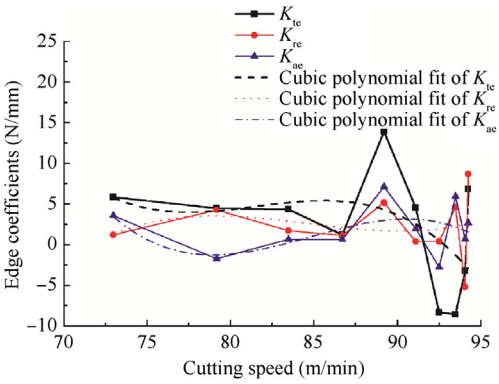

(b) Edge coefficients

Fig. 7 The relationship between cutting speed and coefficients.

method provides accurate average cutting force prediction, but the error remains larger for instantaneous forces especially in the peak position. To conclude, conventional identification method does not offer precise prediction in bull-nose milling due to the neglect of cutting speed's influences on the force prediction.

As cutting speeds vary along the tool axis in the toroidal surface, cutting coefficient changes as well. If constant cutting force coefficients are used in force prediction, discrepancies can be larger by bringing error or obstacle for parameter optimization and selections. Detailed information is explored based on the improved identification method by taking influences of speeds into the identification process.

Through experiments and data processing, the general trend of six cutting force coefficients can be drawn up. It is seen that the ploughing coefficients vary in a relative small range while the shearing ones have a larger span. Experiments are sufficient to support coefficient calculations with various cutting depths as horizontal axis and coefficient values as vertical axis. In Fig. 6, K_{te} K_{re} and K_{ae} have small fluctuation ranges compared with those of the shearing coefficients. The phenomena can be explained by metal removal mechanism acting on the rake and flank contact areas. Drastic changes of shearing coefficients in the small axial depth of cut are characterized by the size effect. In addition, the more the cutting experiments with larger range parameters, the more accurate the fitting curves with more cost. Thus, when performing tests, it needs comprehensive consideration and all groups should

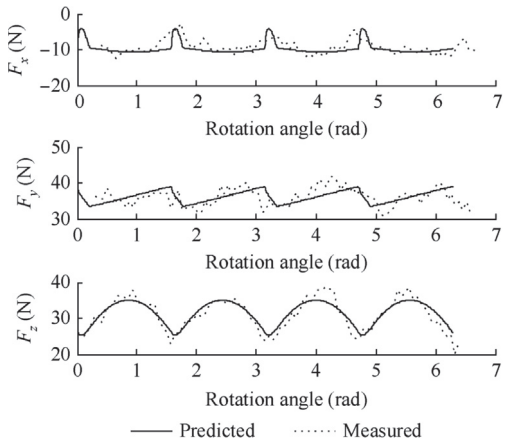

(a) Cutting depth 0.4 mm

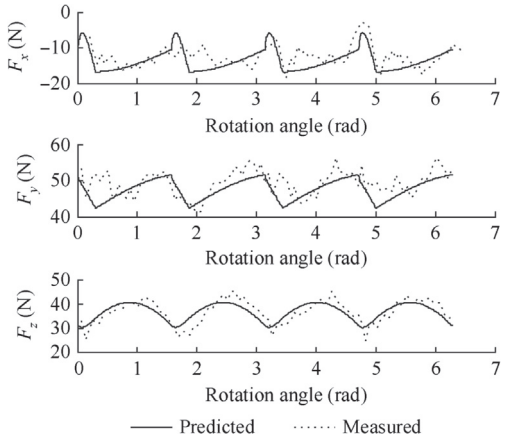

(b) Cutting depth 0.6 mm

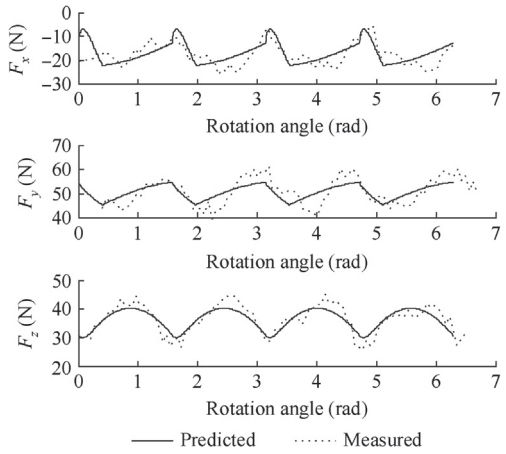

(c) Cutting depth 0.8 mm

Fig. 8 Comparison of cutting forces for down-milling with bull-nose cutter, $s_{tj} = 0.04$ mm/tooth.

satisfy the precision requirements. The coefficients are plotted in Fig. 6(b and d) by using the cubic fitting method.

In Fig. 6, coefficients vary in different cutting depths continuously, and the cutting speed can be calculated by $v = 2\pi r(z)n$, where $r(z)$ is the function of cutting depth and n is the known quantity under certain experiment condition. Therefore, the relations between cutting speeds and coefficients are established during the identification process shown in Fig. 7.

The results of verification are shown in Fig. 8 based on the proposed identification procedure, semi-mechanistic modeling, and then compared with the measured ones. In general, they agree well and show satisfactory prediction in spite of some fluctuations and discrepancies. They may be caused by unstable factors during experiments such as tool wear, vibration, accuracy of the force-measure device, or small error in the adjusting process. Stability lobe diagram (SLD) plots the boundary between stable and unstable cuts as a function of spindle speed and cutting depth. With the aid of SLD, the spindle speed is chosen in the stable zone which has diminutive impact on the system especially in small cutting depths. The whole system presents rigid feature under shallow cutting depth and tool shank distance, so to some extent, tool deflection can be ignored. Although developed hydraulic chucks minimize the runout within 0.02 mm, it still leaves somewhat uneven chip loads among flutes. This kind of load distribution was not considered in simulations but can be involved as illustrated by Wan and Kline.[4,19] The tool used in the tests was newly made, so the degree of tool wear is minimal. Yet as far as what the figures show, F_z has the greatest consistency while some discrepancies exist in x and y directions which do not influence the overall accuracy and trends.

In the machining process, multiple factors are attributed to misalignments between the measured and modeled forces.[20,21] Despite the existence of these factors, the results obtained from experiments and simulations verify the validity of the coefficients identification methods and force models. Fig. 8 illustrates that the largest deviation remains in the range of 25% while the smallest can be in a very close distance within the two curves. The error of the tests is also below 20% in most cases, especially for F_x and F_y cutting force components.

4. Conclusions

Expressions of each discretized force component are derived based on the semi-mechanistic force model, and by integrating the elements along the tool axis, resultant forces are obtained. An improved identification method is then proposed to provide accurate force predictions for bull-nose cutters. Finally, the model and the approach are tested and validated by comparing the experimental results with the simulations.

(1) The traditional coefficient identification method is modified by taking influences of various cutting speeds into the force prediction process. With elevation z as the coefficient-curve horizontal coordinate, it makes the force coefficients prediction more convenient and accurate compared with the traditional method.
(2) Demonstrations through experiments and theoretical derivations are adopted to show validity and effectiveness of the analysis. During the process, six coefficients along the tool axis are illustrated by using the cubic fitting method for given cutting conditions, cutter, and workpiece material. However, it is not limited to specific types and the fitting procedure is determined by real experimental data.

(3) It is shown that the results predicted by the force model and coefficient identification approach correspond well with the experiment outcomes. The method can also be further employed in cutting force predictions with certain inclination angle or parameter selections.

Acknowledgements

The authors greatly acknowledge the financial support from the Postgraduate Seed Fund of Northwestern Polytechnical University (No. Z2012038), National Natural Science Foundation of China (No. 51005183) and National Key S&T Special Projects (No. 2011X04016-031) to carry out this work.

References

1. Cheng PJ, Tsay JT. A study on instantaneous cutting force coefficients in face milling. *Int J Mach Tools Manuf* 1997;**37**(10):1393–408.
2. Gonzalo O, Beristain J. A method for the identification of the specific force coefficients for mechanistic milling simulation. *Int J Mach Tools Manuf* 2010;**50**(9):765–74.
3. Wang JJJ, Zheng CM. Identification of shearing and ploughing cutting constants from average forces in ball-end milling. *Int J Mach Tools Manuf* 2002;**42**(6):695–705.
4. Wan M, Zhang WH. Efficient calibration of instantaneous cutting force coefficients and run-out parameters for general end mills. *Int J Mach Tools Manuf* 2007;**47**(11):1767–76.
5. Altintas Y, Eynian M. Identification of dynamic cutting force coefficients and chatter stability with process damping. *CIRP Ann Manuf Technol* 2008;**57**(1):371–4.
6. Tukora B, Tibor S. Real-time determination of cutting force coefficients without cutting geometry restriction. *Int J Mach Tools Manuf* 2011;**51**(12):8719.
7. Lee HU, Cho DW. Development of a reference cutting force model for rough milling feed rate scheduling using FEM analysis. *Int J Mach Tools Manuf* 2007;**47**(1):158–67.
8. Engin S, Altintas Y. Mechanics and dynamics of general milling cutters Part I: helical end mills. *Int J Mach Tools Manuf* 2001;**41**(15):2195–212.
9. Gradisek J, Kalveram M. Mechanistic identification of specific force coefficients for a general end mill. *Int J Mach Tools Manuf* 2004;**44**(4):404–14.
10. Zhang L, Zheng L. Prediction of cutting forces in end milling of pockets. *Int J Adv Manuf Technol* 2005;**25**(3):281–7.
11. Zhang L, Zheng L. Prediction of cutting forces in milling of circular corner profiles. *Int J Mach Tools Manuf* 2004;**44**(2–3):225–35.
12. Wang HY, Qin XD. Prediction of cutting forces in helical milling process. *Int J Adv Manuf Technol* 2012;**58**(9–12):849–59.
13. Lee P, Altintas Y. Predictions of ball-end milling forces from orthogonal cutting data. *Int J Mach Tools Manuf* 1996;**36**(9):1059–72.
14. Fontaine M, Devillez A. Predictive force model for ball-end milling and experimental validation with a wavelike form machining test. *Int J Mach Tools Manuf* 2006;**46**(3–4):367–80.
15. Yucesan G, Altintas Y. Prediction of ball end milling forces. *ASME J Eng Ind* 1996;**118**(1):95–103.
16. Cao QY, Zhao J. Force coefficients identification considering inclination angle for ball-end finish milling. *Precis Eng* 2012;**36**(2):252–60.
17. Insperger T, Gradisek J. Machine tool chatter and surface location error in milling processes. *J Manuf Sci Eng* 2006;**128**(4):913–20.
18. Smith S, Tlusty J. An overview of modeling and simulation of the milling process. *Trans ASME J Eng Ind* 1991;**113**(2):169–75.
19. Kline WA, Devor RE. The effect of runout on cutting geometry and forces in end milling. *Int J Mach Tools Manuf* 1983;**23**(2–3):123–40.
20. Li XP, Li HZ. Theoretical modeling of cutting forces in helical end milling with cutter runout. *Int J Mech Sci* 2004;**46**(9):1399–414.
21. Yun W, Guo Q. Numerical simulation and prediction of cutting forces in five-axis milling processes with cutter runout. *Int J Mach Tools Manuf* 2011;**51**(10–11):806–15.

Gao Ge received her B.S. degree from Northwestern Polytechnical University (NWPU) in 2010, and now is a postgraduate. Her main research interest is machining technology.

Zhang Dinghua received his B.S. and M.S. degrees from Northwestern Polytechnical University in 1981 and 1984, respectively. He also received his Ph.D. degree in Aeronautical and Astronautical Manufacturing Engineering from Northwestern Polytechnical University in 1989 and became a professor there in 1991. His main research areas of interest include multi-axis machining, high-speed machining, machining surface integrity, and industrial CT technology.